Hidden early clinopyroxene relicts record reactive porous flow in oceanic plutonic series

Cloé Falc'hun[1]*, Lydéric France[1,2]

1. Université de Lorraine, CRPG, CNRS

2. Institut Universitaire de France (IUF)

*Corresponding author: cloe.falc-hun@univ-lorraine.fr

The present paper is a non-peer reviewed preprint submitted to EarthArXiv. This paper has been submitted at Journal of Petrology, a peer-reviewed journal.

Keywords: mid ocean ridge, crystal mush, differentiation, reactive porous flow, clinopyroxene relicts

Abstract

Almost two-thirds of the Earth's magmatic budget is concentrated at mid-ocean ridges, with 85% of this being emplaced as intrusive rocks. In these systems, now understood to consist mostly of a crystal-dominated igneous medium (mush), melt differentiation at depth is predominantly governed by melt-mush reactions. These reactions have been well described for primitive lithologies (ranging from troctolite to gabbro) and are characterized by disequilibrium processes between a reactive melt and the crystal framework through which it percolates. This leads to mineral assimilation and crystallization reactions. Although thermodynamic and geochemical models (assimilation and fractional crystallization) consistently indicate the need for clinopyroxene assimilation in the case of a gabbroic mush, petrographic observations have only revealed poikilitic and late interstitial clinopyroxene interpreted as a late crystallizing phase. Here, we present chromium and titanium chemical maps of an apparently interstitial poikilitic clinopyroxene from ODP Hole 735B, Southwest Indian Ridge. We present key evidence for Cr-rich amoeboidal clinopyroxene relicts preserved within the larger poikilitic grains. In this reactive context, these primitive relicts are remnants of earlier clinopyroxene assimilation. Accordingly, clinopyroxene may be present early in oceanic plutonic crystallization, at least at slow- and ultraslow-spreading ridges, and it must participate in assimilation reactions occurring during the reactive porous flow differentiation process.

Introduction

The generation of oceanic crust at mid-ocean ridges represents almost two-thirds of the Earth's magmatic budget. Melts erupted along spreading ridge axes (mid-ocean ridge basalts, MORBs) result from the adiabatic melting of the mantle and subsequent differentiation processes during crustal accretion. Therefore, they are key to accessing the composition of the mantle and constraining magma reservoir dynamics. Nonetheless, the precise petrogenesis of MORBs remains only partially quantified.

Although geophysical surveys have highlighted the presence of localized melt-rich lenses, igneous reservoirs are dominantly characterized by crystal mush—a magmatic medium in which interconnected crystals form a rigid framework (Sinton and Detrick, 1992; Canales et al., 2009; Jian et al.; 2017, Dunn et al., 2005). Therefore, fractional crystallization and crystal settling, though commonly invoked, are unlikely to be the sole processes involved in magmatic differentiation. The occurrence of melt-mush reactions *via* reactive porous flow is likely widespread (Dick and Natland, 1996; Coogan et al., 2002; Lissenberg and MacLeod, 2016; Lissenberg et al., 2019; Boulanger et al., 2020; Sanfilippo et al., 2020; Ferrando et al., 2021a; Boulanger & France, 2023). While fractional crystallization defines the liquid line of descent, its chemical disruption (Sanfilippo et al., 2015; Leuthold et al., 2018; Zhang et al., 2020; Boulanger et al., 2021) along with petrographic disequilibrium textures (Lissenberg and Dick, 2008; Lissenberg and MacLeod, 2016; Boulanger et al., 2020) can be used to constrain assimilation/crystallization reactions between the crystal framework and the buoyant reactive melt. The main characteristics of these reactions are, petrographically, textural evidence for the assimilation of olivine and plagioclase and the late crystallization of clinopyroxene, and chemically, the decoupling of major and minor or trace elements in plagioclases (An-La) and clinopyroxenes (Mg#-Ti) (Lissenberg and MacLeod, 2016; Sanfilippo et al., 2020; Boulanger et al., 2020; Ferrando et al., 2021a). Isotopic constraints also support the existence of such open-system processes (McCoy-West et al., 2020).

Thermodynamic and geochemical models of these reactions refine our understanding of reactive porous flow (Boulanger and France, 2023; Gleeson et al., 2023). However, these models have also produced paradoxical findings. Although models in gabbros require clinopyroxene assimilation to reproduce melt and mush-forming minerals trace element composition or to make the process thermodynamically feasible, petrological evidence suggests the late crystallization of this mineral, which is apparently interstitial and lacks any relicts. Early, Cr-rich clinopyroxene cores have been described in plutonic series at various localities (Leuthold et al., 2018; Boulanger et al., 2020); however, their relict nature and potential link with differentiation via reactive porous flow remain difficult to demonstrate directly. Recent work by Ubide et al. (2025) provides evidence supporting the interpretation of such cores as inherited relicts formed in the deep crustal reservoirs.

Here, we report amoeboid clinopyroxene core relicts hidden within large poikilitic grains in gabbros from the Atlantis Bank Oceanic Core Complex (OCC). These relicts record striking evidence of early clinopyroxene assimilation during the formation of oceanic plutonic series.

Geological setting

Poikilitic clinopyroxene hosting plagioclase and olivine chadacrysts are common in oceanic plutonic series (Coogan et al., 2000; Koepke et al., 2011; Gillis et al., 2014; Lissenberg and MacLeod, 2016; Leuthold et al., 2018; Boulanger et al., 2020, 2021; France et al., 2021; Akizawa et al., 2023; Basch et al., 2024). Here, we focus on a typical olivine gabbro from an ultraslow-spreading ridge that was sampled at Atlantis Bank, Southwest Indian Ridge. This gabbro contains large poikilitic clinopyroxenes. Atlantis Bank is an OCC formed by a detachment fault on the eastern flank of the Atlantis II transform fault of the Southwest Indian Ridge (SWIR) (Dick et al., 1991; Ildefonse et al., 2007; Lagabrielle et al., 2015) (Fig. 1). The OCC is the result of a 3 -km uplift of the lower oceanic crust and is therefore predominantly composed of gabbroic

lithologies (Dick et al., 1991; MacLeod et al., 2017). ODP Hole 735B (1,508 m below the sea floor) was drilled into Atlantis Bank in 1980s and 1990s (Legs 118 and 176) (Dick et al., 2000) and is composed of 76% olivine gabbros (Natland et al., 2002). The igneous crust there consists of 200–500-meter-thick tectonomagmatic units that likely represent partial to entire sections of magmatic reservoirs (Dick et al., 2000; Boulanger et al., 2020). At this site, differentiation from olivine-rich troctolite to differentiated oxide gabbros and localized felsic veins is mainly governed by reactive porous flow (Robinson et al., 2000; Dick et al., 2000; Nguyen et al., 2018; H. J. B. Dick et al., 2019; Sanfilippo et al., 2020; Zhang et al., 2020; Boulanger et al., 2020, 2021; Ferrando et al., 2021a; Dhar et al., 2022; Ferrando et al., 2022; Pieterek et al., 2022; Zhang and Liu, 2023). Here, we focus on an olivine gabbro from 74–78 cm depth in section 91R1 (518.15mbsf), from the lower part of the igneous reservoir identified by Boulanger et al. (2020) as having formed by sill stacking. This reservoir was formed by the accumulation of dozens of sills in its lower part (~125 m), through which reactive melt percolated, enabling reactive porous flow. This melt accumulated at the top of these sills to form the upper part of the reservoir (~125 m) (Boulanger et al., 2020). In the relatively primitive lithologies (troctolite and gabbro), the study of textural and geochemical characteristics of olivine, plagioclase, and clinopyroxene has revealed assimilation/crystallization reactions (e.g., $Ol_1 + Pl_1 + melt_1 = Ol_2 + Pl_2 + Cpx + melt_2$ and $Ol + Pl_1 + Cpx_1 + melt_1 = Pl_2 + Cpx_2 + melt_2$) (Sanfilippo et al., 2020; Zhang et al., 2020; Boulanger et al., 2020, 2021; C. Ferrando et al., 2021a; Zhang and Liu, 2023).

Methods

We combined major, minor, and trace element maps with *in situ* quantitative measurements, all acquired using a JEOL JXA 8230 electron microprobe at the CRPG (Nancy, France). X-ray maps of major and minor element concentrations in clinopyroxene were acquired using a high-current electron beam operating at 15 keV, 500 nA, with a 4 µm probe diameter and a dwell time of 200 ms. The following crystals were used

for trace element acquisition: PETJ for Ti, PETL for Cr, and three PETH crystals for P. Na, Mg, Al, Fe, Si, S, Ca, and Cl were simultaneously analyzed by energy-dispersive X-ray spectroscopy (EDS). Higher-resolution zoomed-in maps were obtained for specific areas (Fig. 2C). The settings were adjusted to optimize the signal for the elements of interest in each mineral. Zoomed-in areas of the clinopyroxenes were analyzed at 15 keV, 500 nA, with a 2 µm probe diameter and a dwell time of 100 ms; in those cases, we used a TAP crystal for Al, PETL for Cr, PETH for Ca, PETH for Ti, and PETH for P, with Mg, Fe, Si, and S analyzed by EDS. High-resolution maps of olivine were obtained using a high-current electron beam operating at 15 keV, 500 nA, with a 2 µm probe diameter and a dwell time of 200 ms; for these maps, we used a TAP crystal for Al, one PETL and two PETH crystals for P, and PETH for Ca, with Mg, Fe, Si, and S were analyzed by EDS. All the maps are semi-quantitative; peak positions were adjusted for each of them using natural and synthetic minerals.

Quantitative *in situ* analyses were performed using an electron beam operating at 15 keV, 15 nA, and with a 1 µm probe diameter. The on-peak and background counting times were respectively: 10 and 5 s for Na, K, and P; 20 and 10 s for Si, Al, Mg, and Fe; 20 and 20 s for Ti; 40 and 20 s for Ca, Cr, and Mn; and 60 and 30 s for Ni. Five crystals were used: TAPH for Na and Mg; LIFH for Fe, Ni, and Mn; PETH for K and Ti; TAP for Si and Al; and PETL for P, Ca and Cr (Table S1). The calibration standards were as follows: MongOLSh11-2 olivine (Batanova et al., 2019) for Si and Mg, Al_2O_3 from Micro-analysis consultants, LTD (MAC) for Al, Cr-diopside (MAC) for Ca, chromite from the Smithsonian (SM; Jarosewich et al., 1980) for Cr, anorthoclase (SM) for Na, fayalite (SM) for Fe, NiO (MAC) for Ni, rhodonite (MAC) for Mn, orthoclase Berlin provided by ETH Zurich for K, apatite (MAC) for P, and rutile (MAC) for Ti. These standards were also analyzed regularly throughout the analytical sessions (Table S3). The standard error obtained for these analyses ranges from 0.013 to 0.014 wt.% for Cr, 0.012 to 0.019 wt.% for Ti, and 0.21 to 0.22 for Mg#.

Results

Following extensive detailed studies of the Atlantis Bank OCC plutonic series by our group (Nguyen et al., 2018; Dick et al., 2019; Boulanger et al., 2020, 2021; Ferrando et al., 2021a; Ferrando et al., 2021b; Dhar et al., 2022, 2025; Pieterek et al., 2022; Boulanger and France, 2023) and others (Dick et al., 2000; Natland and Dick, 2001; Robinson et al., 2000; Sanfilippo et al., 2020; Zhang et al., 2020; Zhang and Liu, 2023), we selected a texturally representative poikilitic olivine gabbro for high-resolution chemical mapping (other examples are presented in Supplementary data Fig. S2 as well as dataset Table S4 of all the maps from Fig.2 and 3 and the quantitative data Table S2). Here, we focus on a single poikilitic clinopyroxene crystal enclosing rounded olivines and partially resorbed plagioclases (Fig. 2A, B & S1). We identified 3 compositionally distinct domains within optically continuous clinopyroxene oikocrysts based on Cr_2O_3, TiO_2, and Mg#. The "Cr-domain" is enriched in Cr_2O_3 (0.88–1.00 wt.%) and relatively depleted in TiO_2 (0.42–0.97 wt.%)(Fig. 2C) compared to the rest of the crystal, which is Ti-rich (1.10–1.44 wt.%) (Fig. 3C, D). The primitive Cr domains are dispersed within the larger Ti-rich late-stage oikocryst and appear similar to inherited cores (Fig. 2A, B).

High-resolution chemical maps of these areas reveal two chemically distinct domains within the surrounding Ti-rich part of the crystal (Fig. 3C, D). The "Ti-domain" is quantitatively the main part enriched in TiO_2 (1.10–1.44 wt.%) and depleted in Cr_2O_3 (0.72–0.89 wt.%). It surrounds the primitive Cr domains and has a xenomorphic shape. The "Cr-Ti domain" is the second Ti-rich domain enriched in TiO_2 (1.15–1.54 wt.%) and in Cr_2O_3 (0.82–0.96 wt.%) (Fig. 3C, D). When present, it occurs near grain boundaries. The studied clinopyroxene has high Mg# values (molar ratio $[Mg/(Mg + Fe_{tot})] \times 100$) ranging from 85.6 to 89.6, which increase overall from the core to the rim. The Mg# of Cr domains ranges from 85.6 to 88.3, while it ranges from 88.5 to 89.1 for Ti domains, and from 88.4 to 89.6 for Cr-Ti domains. The highest Mg# values occur in the TiO_2-enriched zones, regardless of Cr content (i.e., for both Ti and Cr-Ti domains; Fig. 3C, D). Similar observations were made in other samples (Fig. S2).

Olivine chadacrysts are rounded and in contact with all three chemical domains identified in clinopyroxene (Fig. 2C); some are locally enclosed within the early Cr domains (Fig. 2C). Since the incorporation of phosphorus into olivine is enhanced during fast crystal growth (e.g., Milman-Barris et al., 2008; Welsch et al., 2014; Shea et al., 2019), and because the low diffusion rate of phosphorus in olivine allows the preservation of early chemical heterogeneities (Nelson et al., 2024), initially skeletal and dendritic olivine morphologies can be tracked by quantifying phosphorus zonation (Milman-Barris et al., 2008; Welsch et al., 2013; Xing et al., 2017; Lang et al., 2021; Mourey et al., 2023a; , 2023b). Here, although the olivine grains are rounded to subhedral, phosphorus chemical maps highlight localized enrichments which mimic repetitive crystal growth fronts. These enriched zones are truncated by less enriched areas, resembling the rims of the olivines. The grains themselves display rounded morphologies.

Discussion

Solidification of an oceanic poikilitic olivine gabbro: Snapshot of a reactive mush

The igneous texture studied here is typical of gabbros found at slow-spreading ridges, with clinopyroxene mainly present as oikocrysts enclosing olivine and plagioclase chadacrysts (Lissenberg and Dick, 2008; Leuthold et al., 2018; Boulanger et al., 2021; Ferrando et al., 2021a). Such assemblages have been extensively described and interpreted to document a crystallization sequence in which olivine and plagioclase form and react with an ascending melt, leading to the formation of late interstitial clinopyroxene (e.g., Boulanger et al., 2020). The preserved domains highlighted by chemical maps allow us to track the various stages of crystallization, from the early phases' precipitation to the later stage melt-mush reactions. Early skeletal olivine morphologies, as seen in phosphorus zonation indicate an early episode of rapid growth (Fig. 3A, B & Fig. 4 step 1) (Welsch et al., 2014). P-poor overgrowths on complex olivine cores are observed in most olivine chadacrysts, highlighting that the initial skeletal textures ripened

once crystallization conditions were closer to equilibrium. The localized truncation of several skeletal growth faces also highlights that dissolution/assimilation occurred first after the initial growth and ripening stage (Fig. 3A; step 2), whereas their rounded final shapes indicate subsequent crystallization, followed by a second step of partial assimilation (Figs. 2C, 3A; step 3+4). Since these olivine grains are included within the large clinopyroxene oikocryst, even within the earliest formed Cr domains (Fig. 2C), this multistep history of olivine grains must have occurred early, before clinopyroxene crystallization. Rounded olivines are also found within plagioclase grains. The mush may thus have passed through a troctolitic stage before reaching its current gabbroic state (Fig. 2C). The observed assimilation of olivine and the crystallization of plagioclase and clinopyroxene are consistent with the reservoir model of Boulanger et al. (2020) at Atlantis Bank (SWIR) (Fig. 2C), and other crustal sections of slow-spreading ridges (Robinson et al., 2000; Lissenberg and Dick, 2008; Sanfilippo et al., 2015).

High Mg# values in clinopyroxene, as measured in the studied grain, can be explained by its early appearance in the high-pressure crystallization sequence expected from fractional crystallization (Morse, 1980; Grove et al., 1992; Villiger et al., 2007; Ubide et al., 2025). However, this cannot be invoked here because, texturally, clinopyroxene cannot have crystallized before olivine. Indeed, the olivine included in the Cr domain had already undergone several stages of evolution prior to their entrapment in clinopyroxene: fast growth, ripening, and assimilation (Fig.2C, 3B & 4 step 1+2). Thus, the first formed olivine grains certainly contributed to a partial decrease in MgO in the melt before clinopyroxene crystallization, while an Mg increase likely resulted from subsequent olivine partial assimilation (rounded olivines). The Cr domains of clinopyroxene thus crystallized from a relatively primitive melt (Cr-rich) that had likely gained magnesium through olivine assimilation (Figs. 2C, 3C & 4 step 2+3). Although related to large poikilitic clinopyroxene grains that seems to form late in the solidification history, those clinopyroxene Cr domains clearly highlight that clinopyroxene crystallization initiates early in the solidification sequence. The subsequent Ti and Mg increase towards Ti and Cr-Ti domains cannot be

reconciled by further olivine and clinopyroxene crystallization. Alternatively, this could be achieved if a differentiating melt, enriched in incompatible elements (e.g., Ti) mainly through the crystallization of plagioclase and clinopyroxene (Fig. 3C&D), partially react *via* reactive porous flow with the Mg-rich crystal mush cumulus phases (e.g., olivine and clinopyroxene). This model explains why both Ti content and Mg# increase simultaneously in the Ti and Cr-Ti domains of clinopyroxene (Fig. 3C & 4 step 4'). Such a decoupling between compatible and incompatible elements is typical of reactive systems (Lissenberg and Dick, 2008; Sanfilippo et al., 2015; Lissenberg and MacLeod, 2016; Boulanger et al., 2020). The most external parts of the clinopyroxene also locally contain interstitial zones that are enriched in both Ti and Cr (Cr-Ti domains), which likely formed late, from interstitial melts (Fig. 4 step 5). In oceanic gabbros, late interstitial melts are commonly depleted in Mg and Cr, and strongly enriched in Ti, thus crystallizing Fe-Ti oxides and amphibole (e.g., Koepke et al., 2018). Here, the concomitant enrichment of Ti, Cr, and Mg in late interstitial clinopyroxenes highlights the ultimate involvement and recharge of relatively primitive melts (Mg- and Cr-rich) that likely percolated interstitially and interacted with either evolved (Ti-rich) interstitial melts or Fe-Ti oxides (Fig. 4 step 5). Alternatively, the percolation of Ti-rich interstitial melt through primitive, Mg- and Cr-rich cumulus phases, like olivine and clinopyroxene, could explain such joint Cr-Ti-Mg enrichments (e.g., Lissenberg and MacLeod, 2016; Ubide et al., 2025). In any case, the signatures of clinopyroxene rims clearly document extensive melt-mush interactions in a reactive porous flow.

Amoeboid-shaped clinopyroxene core: Evidence for early assimilation in an oceanic plutonic series

Accretion and differentiation models of the lower oceanic plutonic crust involve reactive porous flow (Dick and Natland, 1996; Coogan et al., 2002; Lissenberg et al., 2019; Sanfilippo et al., 2020; Boulanger et al., 2020; Ferrando et al., 2021a). Although most thermodynamic and AFC models require some clinopyroxene assimilation (e.g., Boulanger and France, 2023; Gleeson et al., 2023), demonstrating this reaction in natural

222 samples remains challenging. Poikilitic clinopyroxenes are usually interpreted as representing one of the
223 latest crystallized phases to form, usually after the cumulus minerals (olivine and plagioclase) in the
224 oceanic igneous series. Here, however, although the studied poikilitic clinopyroxene appears, based on
225 textural relationships, to be a late phase at first glance (Fig. 2A, B), it contains several apparently isolated
226 Cr-rich and Ti-poor domains (Cr domains) that we interpret as having formed early from a relatively
227 primitive mafic melt (Fig. 2C). Since these domains are in optical continuity with the larger oikocryst, and
228 are thus part of the same single crystal, it is unlikely that they crystallized independently and became
229 perfectly aligned during the progressive crystallization of a more evolved, Cr-depleted, and Ti-enriched
230 melt. Instead, our results imply that these Cr-rich domains represent a single, early clinopyroxene grain,
231 and the domains are connected in 3D. This, in turn, implies that the 3D morphology of this early Cr-rich
232 clinopyroxene is amoeboidal, with the various domains being only apparently isolated by sectioning (Fig.
233 4 step 4).

234 The origin of such an amoeboidal grain must clearly be related to the dissolution (or assimilation)
235 of an earlier, larger Cr-rich grain whose initial morphology is no longer preserved. This early Cr-rich
236 clinopyroxene assimilation is potentially associated with partial olivine and plagioclase assimilation by a
237 reactive melt. It preceded the crystallization of Cr-poor and Ti-rich clinopyroxene mantles/rims that likely
238 partially fill the intragrain space formerly occupied by interstitial melt (Fig. 4 steps 4 & 4'). These rims also
239 have a high Mg#, strongly suggesting that they formed from a melt that had reacted with a mafic mush.
240 Such simultaneous Ti-Mg enrichments in clinopyroxenes are commonly observed in lithologies affected by
241 reactive processes (Lissenberg and Dick, 2008; Yang et al., 2019). Subsequent crystallization was likely
242 dominated by Cr-poor and Ti-rich clinopyroxene growth (Ti domains), which, along with progressive
243 differentiation, eventually produced the observed poikilitic texture (Fig. 4). Locally, an additional stage of
244 relatively primitive melt infiltration into a melt-poor mushy domain likely formed the interstitial Cr-, Mg-,
245 and Ti-rich external rims (Cr-Ti domains) (Fig.4 step 5). Therefore, our results strongly support the presence

of Cr-rich, Ti-poor clinopyroxene early in the crystallization sequence of oceanic mafic mushes, as well as their participation as reactants (along with olivine and plagioclase) in the reactions involved in reactive porous flow, the main differentiation process in such igneous series. Those Cr-rich clinopyroxene being themselves formed after a reactive stage that partially dissolved early olivine grains, we eventually highlight herein that the entire solidification sequence is interrupted by several successive stages of crystal partial dissolution (Fig.3, 4; steps 2, 4, 5) in relation with melt recharges (i.e. reactive porous flow). In the present case, although clinopyroxene is not the first cumulus mineral to form (Fig.4 steps 1-3), its early crystallization in the solidification sequence may partially explain the pyroxene paradox. The latter concept relies on the identification that MORB signatures reflect early clinopyroxene fractionation, although their phenocryst load is dominated by plagioclase and olivine (Francis, 1986), and despite the texture of plutonic oceanic rocks points to the late crystallization of interstitial clinopyroxenes (Ubide et al., 2025). Here Cr-rich clinopyroxene domains support the early formation of such minerals.

Conclusions

Our study of a representative poikilitic olivine gabbro from the Atlantis Bank oceanic core complex (Southwest Indian Ridge), based on unique chemical maps, reveals a striking feature: a co-enrichment of Mg and Ti from the core to the rim. This pattern cannot be explained by classical crystallization processes or magma mixing. Using Cr-Ti-Mg systematics, in a single large poikilitic clinopyroxene grain, we identified both the presence of a primitive Cr-rich, Ti-poor amoeboidal, partially resorbed clinopyroxene core and subsequent clinopyroxene overgrowths that formed *via* reactive porous flow. The morphology of the clinopyroxene core attests for the first time to its involvement as a reactant in assimilation reactions, consistent with previous thermodynamic and geochemical models requiring clinopyroxene as an early phase, whereas most petrological observations have relegated clinopyroxene crystallization to later stages

in such settings. Early Cr-rich clinopyroxenes are therefore present in the initial mushy assemblages of oceanic crust and participate as reactants (with olivine and plagioclase) in melt-mush reactions that govern magmatic differentiation at slow-spreading ridges. This study highlights the added value of using high-resolution chemical maps to reveal cryptic mineral histories and study complex petrological processes. Beyond this specific case, our approach reveals multiple stages of melt-mush reactions during oceanic plutonic series solidification. This provides more detailed insights into the evolution of magmatic reservoirs and the interpretation of geochemical signatures in both plutonic and volcanic sections of the oceanic crust.

Acknowledgments

This research was supported by CNRS-INSU, IODP-France, and by the French National Research Agency (ANR) through the project MUSH-OCEAN (ANR-23-CE49-013; P.I., Lydéric France). This is CRPG contribution number xxxx and MUSH-OCEAN contribution number xx.

References

Akizawa, N., Godard, M., Ildefonse, B., Arai, S., 2023. Formation of lower fast-spread oceanic crust: a structural and geochemical study of troctolites in the Hess Deep Rift (East Pacific Rise). Prog. Earth Planet. Sci. 10, 30. https://doi.org/10.1186/s40645-023-00560-4

Basch, V., Sanfilippo, A., Snow, J.E., Loocke, M., Zanetti, A., 2024. Accretion of the Lower Oceanic Crust at Fast-Spreading Ridges: Insights from Hess Deep (East Pacific Rise, IODP Expedition 345). J. Petrol. 65, egae048. https://doi.org/10.1093/petrology/egae048

Batanova, V.G., Thompson, J.M., Danyushevsky, L.V., Portnyagin, M.V., Garbe-Schönberg, D., Hauri, E., Kimura, J., Chang, Q., Senda, R., Goemann, K., Chauvel, C., Campillo, S., Ionov, D.A., Sobolev, A.V., 2019. New Olivine Reference Material for *In Situ* Microanalysis. Geostand. Geoanalytical Res. 43, 453–473. https://doi.org/10.1111/ggr.12266

Boulanger, M., France, L., 2023. Cumulate Formation and Melt Extraction from Mush-Dominated Magma Reservoirs: The Melt Flush Process Exemplified at Mid-Ocean Ridges. J. Petrol. 64, egad005. https://doi.org/10.1093/petrology/egad005

Boulanger, M., France, L., Deans, J.R.L., Ferrando, C., Lissenberg, C.J., Von Der Handt, A., 2020. Magma Reservoir Formation and Evolution at a Slow-Spreading Center (Atlantis Bank, Southwest Indian Ridge). Front. Earth Sci. 8, 554598. https://doi.org/10.3389/feart.2020.554598

Boulanger, M., France, L., Ferrando, C., Ildefonse, B., Ghosh, B., Sanfilippo, A., Liu, C. -Z., Morishita, T., Koepke, J., Bruguier, O., 2021. Magma-Mush Interactions in the Lower Oceanic Crust: Insights From Atlantis Bank Layered Series (Southwest Indian Ridge). J. Geophys. Res. Solid Earth 126, e2021JB022331. https://doi.org/10.1029/2021JB022331

Canales, J.P., Dunn, R.A., Arai, R., Sohn, R.A., 2017. Seismic imaging of magma sills beneath an ultramafic-hosted hydrothermal system. Geology 45, 451–454. https://doi.org/10.1130/G38795.1

Canales, J.P., Nedimovic´, Kent, Carbotte, Detrick, 2009. Seismic reflection images of a near-axis melt sill within the lower crust at the Juan de Fuca ridge | Nature [WWW Document]. URL https://www.nature.com/articles/nature08095 (accessed 2.11.25).

Coogan, L.A., Gillis, K.M., MacLeod, C.J., Thompson, G.M., Hékinian, R., 2002. Petrology and geochemistry of the lower ocean crust formed at the East Pacific Rise and exposed at Hess Deep: A synthesis and new results. Geochem. Geophys. Geosystems 3, 1–30. https://doi.org/10.1029/2001GC000230

Coogan, L.A., Saunders, A.D., Kempton, P.D., Norry, M.J., 2000. Evidence from oceanic gabbros for porous melt migration within a crystal mush beneath the Mid-Atlantic Ridge. Geochem. Geophys. Geosystems 1. https://doi.org/10.1029/2000GC000072

Dhar, A., Ghosh, B., Bandyopadhyay, D., Morishita, T., Tamura, A., France, L., Nguyen, D.K., Boulanger, M., Koley, M., Roy, S., Chattopadhaya, S., 2022. The lower oceanic crust at ultraslow-spreading Southwest Indian Ridge: The inside story. Gondwana Res. 111, 223–248. https://doi.org/10.1016/j.gr.2022.08.008

Dhar, A., Ghosh, B., Morishita, T., Chattopadhaya, S., Bandyopadhyay, D., Rao, N.V.C., France, L., Nguyen, D.K., Roy, S., Koley, M., 2025. Development of oxy-symplectites in a slow-spreading lower oceanic crust: Insights from the Atlantis Bank Gabbro Massif, Southwest Indian Ridge. Am. Mineral. 110, 776–790. https://doi.org/10.2138/am-2024-9350

Dick, H.J., Natland, J.H., 1996. LATE-STAGE MELT EVOLUTION AND TRANSPORT IN THE SHALLOW MANTLE BENEATH THE EAST PACIFIC RISE, Proceedings of the Ocean Drilling Program. Ocean Drilling Program. https://doi.org/10.2973/odp.proc.sr.147.1996

Dick, Henry J. B., Kvassnes, A.J.S., Robinson, P.T., MacLeod, C.J., Kinoshita, H., 2019. The Atlantis Bank Gabbro Massif, Southwest Indian Ridge. Prog. Earth Planet. Sci. 6, 64. https://doi.org/10.1186/s40645-019-0307-9

Dick, H. J. B., MacLeod, C.J., Blum, P., Abe, N., Blackman, D.K., Bowles, J.A., Cheadle, M.J., Cho, K., Ciazela, J., Deans, J.R., Edgcomb, V.P., Ferrando, C., France, L., Ghosh, B., Ildefonse, B., John, B., Kendrick, M.A., Koepke, J., Leong, J. a. M., Liu, C., Ma, Q., Morishita, T., Morris, A., Natland, J.H., Nozaka, T., Pluemper, O., Sanfilippo, A., Sylvan, J.B., Tivey, M.A., Tribuzio, R., Viegas, G., 2019. Dynamic Accretion Beneath a Slow-Spreading Ridge Segment: IODP Hole 1473A and the Atlantis Bank Oceanic Core Complex. J. Geophys. Res. Solid Earth 124, 12631–12659. https://doi.org/10.1029/2018JB016858

Dick, H.J.B., Natland, J.H., Alt, J.C., Bach, W., Bideau, D., Gee, J.S., Haggas, S., Hertogen, J.G.H., Hirth, G., Holm, P.M., Ildefonse, B., Iturrino, G.J., John, B.E., Kelley, D.S., Kikawa, E., Kingdon, A., LeRoux, P.J., Maeda, J., Meyer, P.S., Miller, D.J., Naslund, H.R., Niu, Y.-L., Robinson, P.T., Snow, J., Stephen, R.A., Trimby, P.W., Worm, H.-U., Yoshinobu, A., 2000. A long in situ section of the lower ocean crust: results of ODP Leg 176 drilling at the Southwest Indian Ridge. Earth Planet. Sci. Lett. 179, 31–51. https://doi.org/10.1016/S0012-821X(00)00102-3

Dick, H.J.B., Schouten, H., Meyer, P.S., Gallo, D.G., Bergh, H., Tyce, R., Patriat, P., Johnson, K., Snow, J., Fisher, A., 1991. Proceedings of the Ocean Drilling Program, 118 Scientific Results, Proceedings of the Ocean Drilling Program. Ocean Drilling Program. https://doi.org/10.2973/odp.proc.sr.118.1991

Falloon, T.J., Green, D.H., 1987. Anhydrous partial melting of MORB pyrolite and other peridotite compositions at 10 kbar: Implications for the origin of primitive MORB glasses. Mineral. Petrol. 37, 181–219. https://doi.org/10.1007/BF01161817

Ferrando, Carlotta, Basch, V., Ildefonse, B., Deans, J., Sanfilippo, A., Barou, F., France, L., 2021. Role of compaction in melt extraction and accumulation at a slow spreading center: Microstructures of olivine gabbros from the Atlantis Bank (IODP Hole U1473A, SWIR). Tectonophysics 815, 229001. https://doi.org/10.1016/j.tecto.2021.229001

Ferrando, C., France, L., Basch, V., Sanfilippo, A., Tribuzio, R., Boulanger, M., 2021. Grain Size Variations Record Segregation of Residual Melts in Slow-Spreading Oceanic Crust (Atlantis Bank, 57°E Southwest Indian Ridge). J. Geophys. Res. Solid Earth 126, e2020JB020997. https://doi.org/10.1029/2020JB020997

Ferrando, C., Tribuzio, R., Lissenberg, C.J., France, L., MacLeod, C.J., Basch, V., Villeneuve, J., Deloule, E., Sanfilippo, A., 2022. Brown Amphibole as Tracer of Tectono-Magmatic Evolution of the Atlantis Bank Oceanic Core Complex (IODP Hole U1473A). J. Petrol. 63, egac089. https://doi.org/10.1093/petrology/egac089

France, L., Charvet, V., Toussaint, A., 2025. Advances in Igneous Petrology: Coupling Chemical Maps with Thermodynamic Models to Tackle Mush Crystallization Dynamics and Crystal–Melt Segregation. J. Petrol. 66, egaf044. https://doi.org/10.1093/petrology/egaf044

Francis, D., 1986. The pyroxene paradox in MORB glasses—a signature of picritic parental magmas? Nature 319, 586–589. https://doi.org/10.1038/319586a0

Gleeson, M.L.M., Lissenberg, C.J., Antoshechkina, P.M., 2023. Porosity evolution of mafic crystal mush during reactive flow. Nat. Commun. 14, 3088. https://doi.org/10.1038/s41467-023-38136-x

Grove, T.L., Kinzler, R.J., Bryan, W.B., 1992. Fractionation of mid-ocean ridge basalt (MORB). Geophys. Monogr. Ser. 71, 281–310. https://doi.org/10.1029/GM071p0281

Ildefonse, B., Blackman, D.K., John, B.E., Ohara, Y., Miller, D.J., MacLeod, C.J., Integrated Ocean Drilling Program Expeditions 304/305 Science Party, 2007. Oceanic core complexes and crustal accretion at slow-spreading ridges. Geology 35, 623. https://doi.org/10.1130/G23531A.1

Jarosewich, E., Nelen, J. a., Norberg, J.A., 1980. Reference Samples for Electron Microprobe Analysis. Geostand. Newsl. 4, 43–47. https://doi.org/10.1111/j.1751-908X.1980.tb00273.x

Jian, H., Singh, S.C., Chen, Y.J., Li, J., 2017. Evidence of an axial magma chamber beneath the ultraslow-spreading Southwest Indian Ridge. Geology 45, 143–146. https://doi.org/10.1130/G38356.1

379 Koepke, J., France, L., Müller, T., Faure, F., Goetze, N., Dziony, W., Ildefonse, B., 2011. Gabbros from IODP
380 Site 1256, equatorial Pacific: Insight into axial magma chamber processes at fast spreading ocean
381 ridges. Geochem. Geophys. Geosystems 12. https://doi.org/10.1029/2011GC003655
382 Lagabrielle, Y., Vitale Brovarone, A., Ildefonse, B., 2015. Fossil oceanic core complexes recognized in the
383 blueschist metaophiolites of Western Alps and Corsica. Earth-Sci. Rev. 141, 1–26.
384 https://doi.org/10.1016/j.earscirev.2014.11.004
385 Lang, S., Mollo, S., France, L., Misiti, V., Nazzari, M., 2021. Kinetic partitioning of major-minor cations
386 between olivine and Hawaiian tholeiitic basalt under variable undercooling and cooling rate
387 conditions. Chem. Geol. 584, 120485. https://doi.org/10.1016/j.chemgeo.2021.120485
388 Leuthold, J., Lissenberg, C.J., O'Driscoll, B., Karakas, O., Falloon, T., Klimentyeva, D.N., Ulmer, P., 2018.
389 Partial Melting of Lower Oceanic Crust Gabbro: Constraints From Poikilitic Clinopyroxene
390 Primocrysts. Front. Earth Sci. 6, 15. https://doi.org/10.3389/feart.2018.00015
391 Lissenberg, C.J., Dick, H.J.B., 2008. Melt–rock reaction in the lower oceanic crust and its implications for
392 the genesis of mid-ocean ridge basalt. Earth Planet. Sci. Lett. 271, 311–325.
393 https://doi.org/10.1016/j.epsl.2008.04.023
394 Lissenberg, C.J., MacLeod, C.J., 2016. A Reactive Porous Flow Control on Mid-ocean Ridge Magmatic
395 Evolution. J. Petrol. 57, 2195–2220. https://doi.org/10.1093/petrology/egw074
396 Lissenberg, C.J., MacLeod, C.J., Bennett, E.N., 2019. Consequences of a crystal mush-dominated magma
397 plumbing system: a mid-ocean ridge perspective. Philos. Trans. R. Soc. Math. Phys. Eng. Sci. 377,
398 20180014. https://doi.org/10.1098/rsta.2018.0014
399 MacLeod, C.J., Dick, H.J.B., Blum, P., 2017. Southwest Indian Ridge Lower Crust and Moho. Proc. Int.
400 Ocean Discov. Program 360. https://doi.org/10.14379/iodp.proc.360.2017
401 McCoy-West, A.J., Millet, M.-A., Burton, K.W., 2020. The Neodymium Stable Isotope Composition of the
402 Oceanic Crust: Reconciling the Mismatch Between Erupted Mid-Ocean Ridge Basalts and Lower
403 Crustal Gabbros. Front. Earth Sci. 8. https://doi.org/10.3389/feart.2020.00025
404 Milman-Barris, M., Beckett, J., Baker, M., Hofmann, A., Morgan, Z., Crowley, M., Vielzeuf, D., Stolper, E.,
405 2008. Zoning of phosphorus in igneous olivine. Contrib. Mineral. Petrol. 155, 739–765.
406 https://doi.org/10.1007/s00410-007-0268-7
407 Morse, S.A., 1980. Basalts and Phase Diagrams. Springer New York, New York, NY.
408 https://doi.org/10.1007/978-1-4612-6081-3
409 Mourey, Adrien J, France, L., Ildefonse, B., Gurenko, A., Laporte, D., 2023. Genesis of Carbonatite at
410 Oldoinyo Lengai (Tanzania) from Olivine Nephelinite: Protracted Melt Evolution and Reactive
411 Porous Flow in Deep Crustal Mushes. J. Petrol. 64, egad084.
412 https://doi.org/10.1093/petrology/egad084
413 Mourey, Adrien J., Shea, T., Hammer, J.E., 2023. Preservation of Magma Recharge Signatures in Kīlauea
414 Olivine During Protracted Storage. J. Geophys. Res. Solid Earth 128, e2022JB025523.
415 https://doi.org/10.1029/2022JB025523
416 Natland, J.H., Dick, H.B.J., Miller, D.J., Von Herzen, R.P. (Eds.), 2002. Proceedings of the Ocean Drilling
417 Program, 176 Scientific Results, Proceedings of the Ocean Drilling Program. Ocean Drilling
418 Program. https://doi.org/10.2973/odp.proc.sr.176.2002
419 Natland, J.H., Dick, H.J.B., 2001. Formation of the lower ocean crust and the crystallization of gabbroic
420 cumulates at a very slowly spreading ridge. J. Volcanol. Geotherm. Res. 110, 191–233.
421 https://doi.org/10.1016/S0377-0273(01)00211-6
422 Nguyen, D.K., Morishita, T., Soda, Y., Tamura, A., Ghosh, B., Harigane, Y., France, L., Liu, C., Natland, J.H.,
423 Sanfilippo, A., MacLeod, C.J., Blum, P., Dick, H.J.B., 2018. Occurrence of Felsic Rocks in Oceanic
424 Gabbros from IODP Hole U1473A: Implications for Evolved Melt Migration in the Lower Oceanic
425 Crust. Minerals 8, 583. https://doi.org/10.3390/min8120583

Pieterek, B., Ciazela, J., Boulanger, M., Lazarov, M., Wegorzewski, A.V., Pańczyk, M., Strauss, H., Dick, H.J.B., Muszyński, A., Koepke, J., Kuhn, T., Czupyt, Z., France, L., 2022. Sulfide enrichment along igneous layer boundaries in the lower oceanic crust: IODP Hole U1473A, Atlantis Bank, Southwest Indian Ridge. Geochim. Cosmochim. Acta 320, 179–206. https://doi.org/10.1016/j.gca.2022.01.004

Robinson, P.T., Dick, H.J.B., Natland, J.H., Alt, J.C., Bach, W., Bideau, D., Gee, J.S., Haggis, S., Hertogen, J., Hirth, G., Holm, P.M., Ildefonse, B., Iturrino, G.J., John, B.E., Kelley, D.S., Kikawa, E., Kingdon, A., LeRoux, P.J., Maeda, J., Meyer, P.S., Miller, D.J., Naslund, H.R., Niu, Y.L., Snow, J., Stephen, R.A., Trimby, P.W., Worm, H.U., Yoshinobu, A., 2000. Lower oceanic crust formed at an ultra-slow-spreading ridge: Ocean Drilling Program Hole 735B, Southwest Indian Ridge, in: Ophiolites and Oceanic Crust: New Insights from Field Studies and the Ocean Drilling Program. Geological Society of America. https://doi.org/10.1130/0-8137-2349-3.75

Sanfilippo, A., MacLeod, C.J., Tribuzio, R., Lissenberg, C.J., Zanetti, A., 2020. Early-Stage Melt-Rock Reaction in a Cooling Crystal Mush Beneath a Slow-Spreading Mid-Ocean Ridge (IODP Hole U1473A, Atlantis Bank, Southwest Indian Ridge). Front. Earth Sci. 8. https://doi.org/10.3389/feart.2020.579138

Sanfilippo, A., Tribuzio, R., Tiepolo, M., Berno, D., 2015. Reactive flow as dominant evolution process in the lowermost oceanic crust: evidence from olivine of the Pineto ophiolite (Corsica). Contrib. Mineral. Petrol. 170, 38. https://doi.org/10.1007/s00410-015-1194-8

Sinton, J.M., Detrick, R.S., 1992. Mid-ocean ridge magma chambers. J. Geophys. Res. Solid Earth 97, 197–216. https://doi.org/10.1029/91JB02508

Ubide, T., Murphy, D.T., Emo, R.B., Jones, M.W.M., Acevedo Zamora, M.A., Kamber, B.S., 2025. Early pyroxene crystallisation deep below mid-ocean ridges. Earth Planet. Sci. Lett. 663, 119423. https://doi.org/10.1016/j.epsl.2025.119423

Villiger, S., Müntener, O., Ulmer, P., 2007. Crystallization pressures of mid-ocean ridge basalts derived from major element variations of glasses from equilibrium and fractional crystallization experiments. J. Geophys. Res. Solid Earth 112. https://doi.org/10.1029/2006JB004342

Welsch, B., Faure, F., Famin, V., Baronnet, A., Bachèlery, P., 2013. Dendritic Crystallization: A Single Process for all the Textures of Olivine in Basalts? J. Petrol. 54, 539–574. https://doi.org/10.1093/petrology/egs077

Welsch, B., Hammer, J., Hellebrand, E., 2014. Phosphorus zoning reveals dendritic architecture of olivine. Geology 42, 867–870. https://doi.org/10.1130/G35691.1

Xing, C.-M., Wang, C., Tan, W., 2017. Disequilibrium growth of olivine in mafic magmas revealed by phosphorus zoning patterns of olivine from mafic–ultramafic intrusions. Earth Planet. Sci. Lett. 479, 108–119. https://doi.org/10.1016/j.epsl.2017.09.005

Yang, A.Y., Wang, C., Liang, Y., Lissenberg, C.J., 2019. Reaction Between Mid-Ocean Ridge Basalt and Lower Oceanic Crust: An Experimental Study. Geochem. Geophys. Geosystems 20, 4390–4407. https://doi.org/10.1029/2019GC008368

Zhang, W.-Q., Liu, C.-Z., 2023. Crust-scale reactive porous flow revealed by the brown amphibole in the IODP hole U1473A gabbros, Southwest Indian Ridge. Lithos 450–451, 107209. https://doi.org/10.1016/j.lithos.2023.107209

Zhang, W.-Q., Liu, C.-Z., Dick, H.J.B., 2020. Evidence for Multi-stage Melt Transport in the Lower Ocean Crust: the Atlantis Bank Gabbroic Massif (IODP Hole U1473A, SW Indian Ridge). J. Petrol. 61, egaa082. https://doi.org/10.1093/petrology/egaa082

Fig. 1. (A) The location of the Atlantis II transform fault. (B) 3D bathymetric image of the Atlantis II transform fault, indicating the location of the Atlantis Bank Core Complex (MacLeod et al., 2017) . (C) Cross-axis schematic view of the magmatic system and crustal architecture at slow-spreading ridges (France et al., 2025).

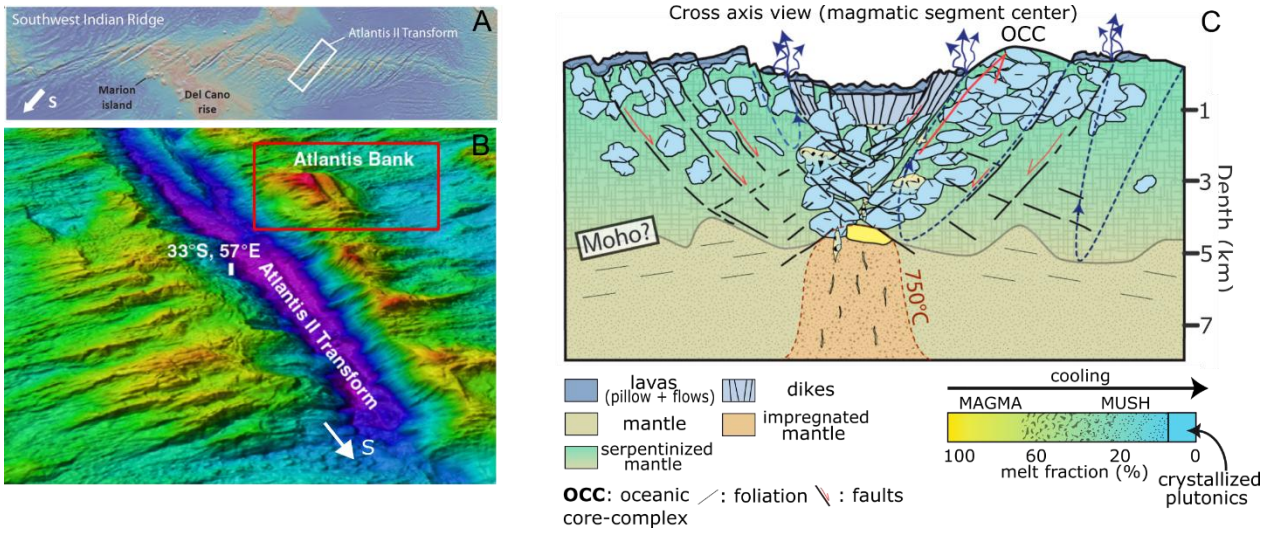

Fig. 2. Single poikilitic clinopyroxene characteristics. (A) Plane-polarized light and (B) cross-polarized light microphotographs of a single poikilitic clinopyroxene engulfing rounded olivines and partially resorbed plagioclases. (C) Ti-Cr map of the clinopyroxene obtained using the Ti/Cr signal ratio, revealing primitive cores, and a modal map of olivine (purple), plagioclase (orange), amphibole and Fe-Ti oxide (red), and sulfide (gray). Dark green (clinopyroxene) and dark purple rectangles (olivine) indicate the locations of enlarged maps presented in Fig. 3. White dashed lines and arrows highlight evidence of assimilation, black dashed line highlights olivine entrapped in the primitive Cr-rich zone (Cr domain).

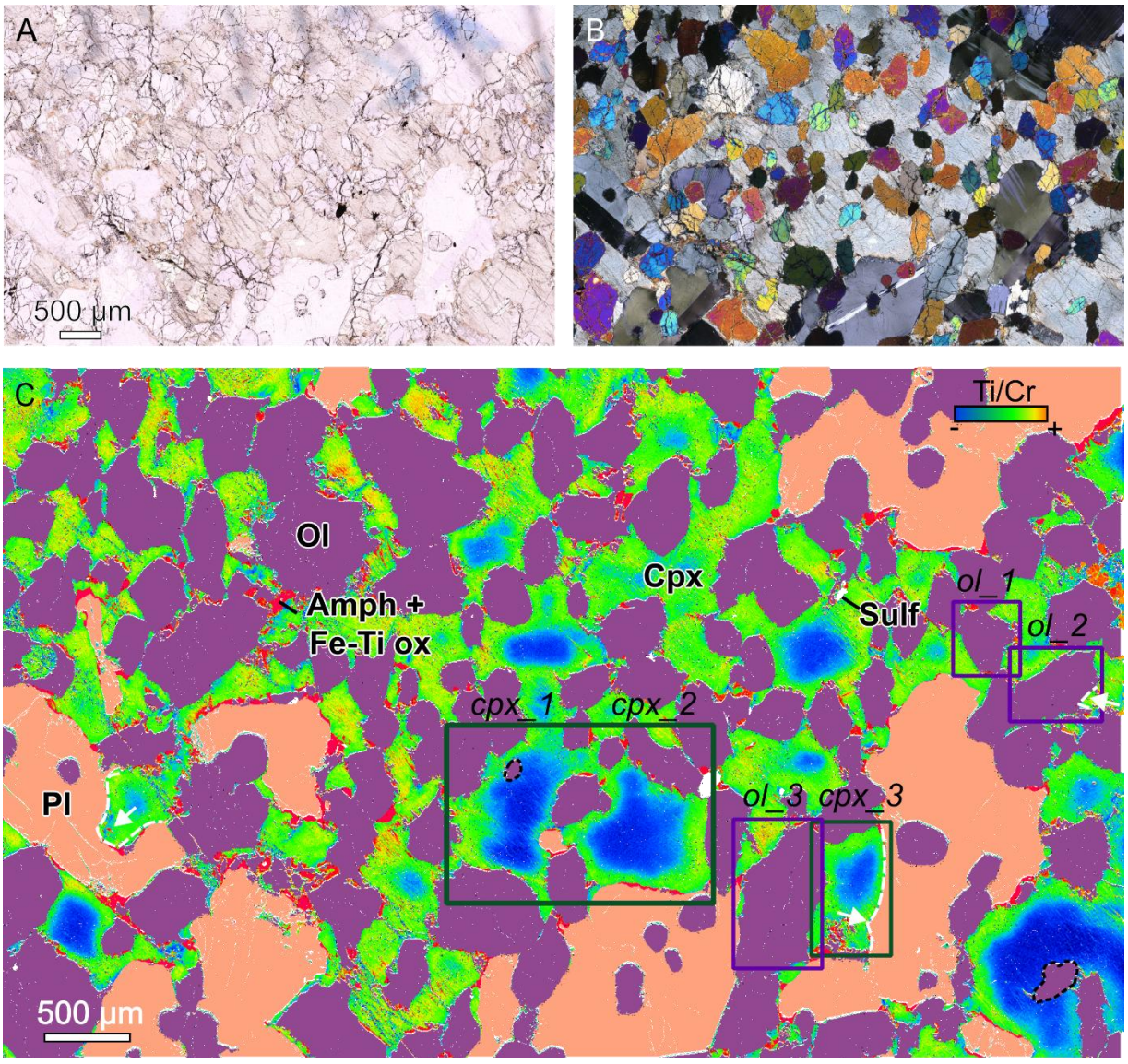
A
500 µm
B
C
Ti/Cr
-
+
Ol
Amph +
Fe-Ti ox
Cpx
Sulf
ol_1
ol_2
cpx_1
cpx_2
Pl
ol_3
cpx_3
500 µm

486

Fig. 3. (A) P maps of olivine chadacrysts within the clinopyroxene oikocryst. Color variations reflect differences in signal intensity, which are given in counts on the scale revealing skeletal relicts indicating initial rapid growth, and (B) an interpretative sketch of the olivine growth process. White dashed lines and arrows highlight evidence of assimilation. All "Steps" refer to those described in Figure 4. The Step 2 box corresponds to the stage occurring between Steps 1 and 3 but not represented in Figure 4. (C) Ti and Cr maps of selected domains of the studied clinopyroxene oikocryst, which show primitive Cr-rich cores (Cr domains) and late Ti-rich rims that are divided in 2 subunits: one internal Cr-poor (Ti domain) and the external Cr-rich (Cr-Ti domain). (D) Point analysis of different locations in each domain of the clinopyroxene (see map locations in Fig. 2C and Fig. S3) compared to data from Boulanger et al. (2020) and to clinopyroxene obtain by fractional crystallization of a primitive melt (Falloon and Green, 1987) through thermodynamic modelling (method in Supplementary Material).

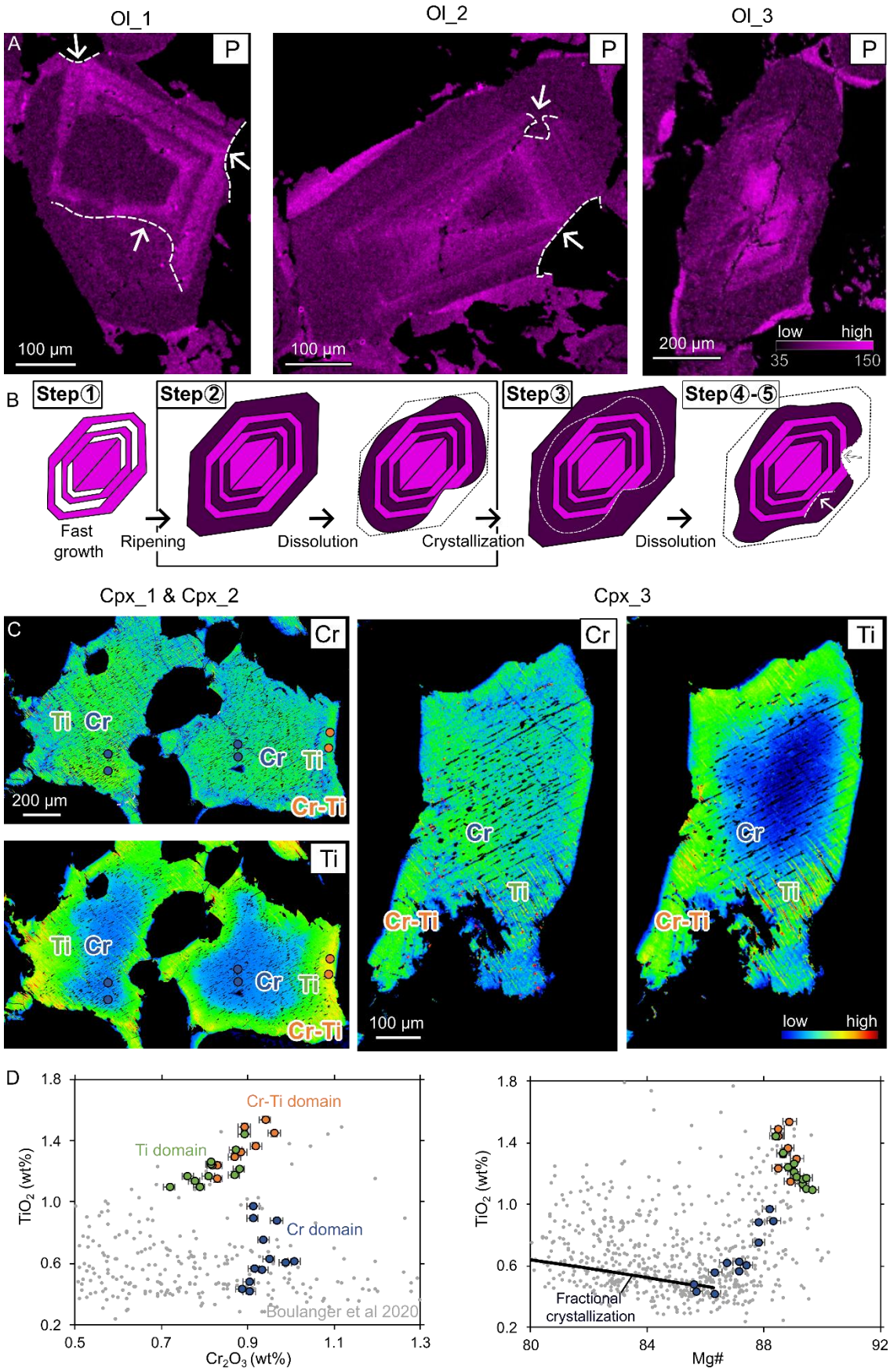
Ol_1
Ol_2
Ol_3
A
P
100 μm
200 μm
low
high
35
150
B
Step①
Step②
Step③
Step④-⑤
Fast growth
Ripening
Dissolution
Crystallization
Dissolution
Cpx_1 & Cpx_2
Cpx_3
C
Cr
Ti
Ti Cr
Cr Ti
Cr-Ti
200 μm
100 μm
low
high
D
Cr-Ti domain
Ti domain
Cr domain
Boulanger et al 2020
TiO2 (wt%)
Cr2O3 (wt%)
Fractional crystallization
Mg#

500

Fig. 4. 3D sketch of the evolution of the main minerals in the studied system (Ol, Pl, Cpx) and some late minerals (amphibole and Fe-Ti oxides), including the olivine fast growth (step 1), the formation of an early Cr-rich clinopyroxene core (step 3), its subsequent partial dissolution to form a residual amoeboidal clinopyroxene (step 4), and later Ti-rich clinopyroxene overgrowths (step 4' and 5), ultimately producing the observed poikilitic texture. 'Prim. melt rich.' denotes a recharge of primitive melt at step 4 and 5. Step 2 corresponds to olivine ripening and partial assimilation (see Fig. 3B). Sections a and b are 2D views of the system along the pink and blue planes, respectively.

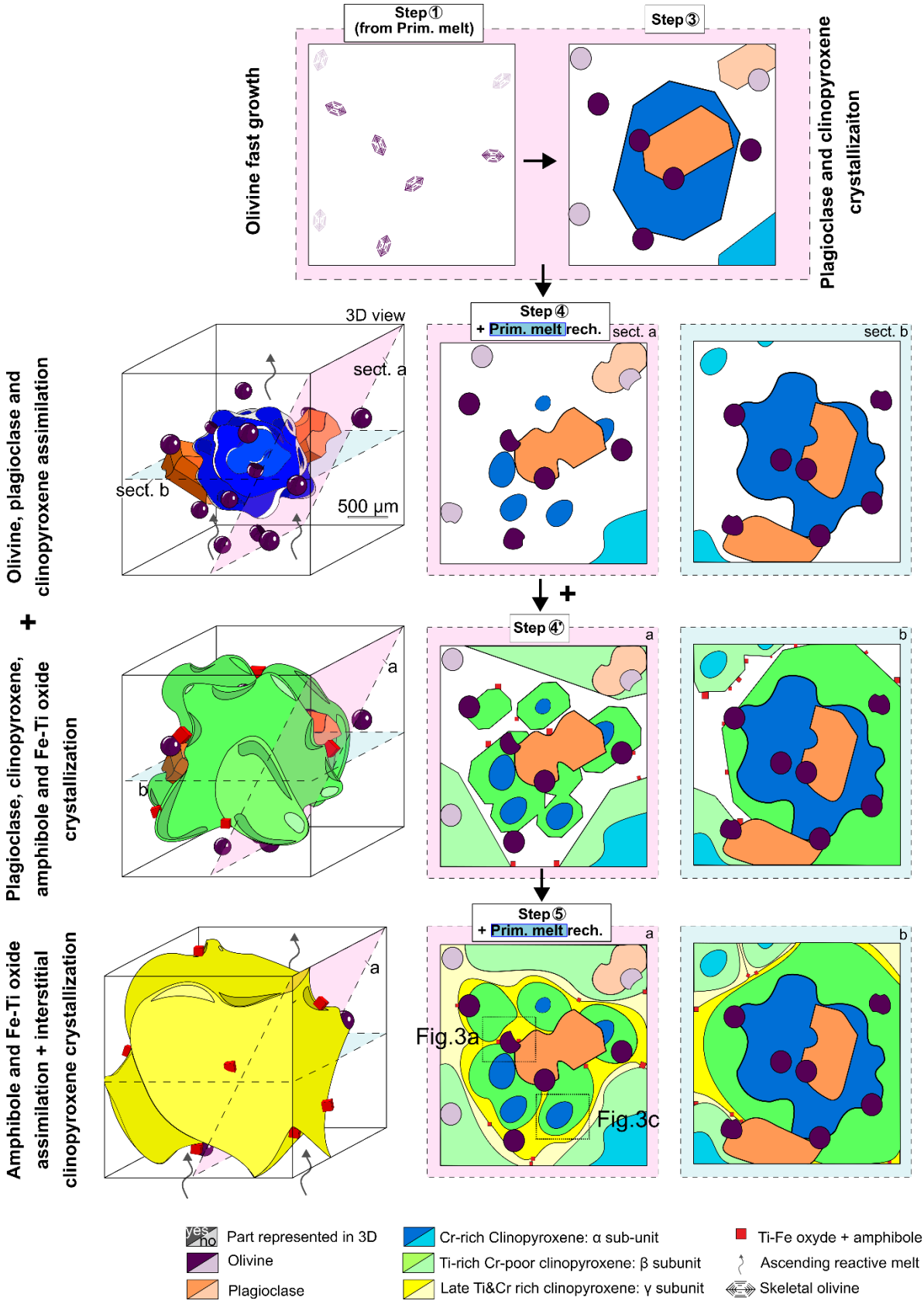
Step① (from Prim. melt)
Step③
Olivine fast growth
Plagioclase and clinopyroxene crystallizaiton
3D view
Step④ + Prim. melt rech.
sect. a
sect. b
500 µm
Olivine, plagioclase and clinopyroxene assimilation
+
Step④'
Plagioclase, clinopyroxene, amphibole and Fe-Ti oxide crystallization
Step⑤ + Prim. melt rech.
Amphibole and Fe-Ti oxide assimilation + interstitial clinopyroxene crystallization
Fig.3a
Fig.3c
Part represented in 3D
Olivine
Plagioclase
Cr-rich Clinopyroxene: α sub-unit
Ti-rich Cr-poor clinopyroxene: β subunit
Late Ti&Cr rich clinopyroxene: γ subunit
Ti-Fe oxyde + amphibole
Ascending reactive melt
Skeletal olivine

509